Effect of ageing on phase evolution and mechanical properties of a high tungsten super-duplex stainless steel

Alfred R. Akisanya[1], Udoka Obi and Neill C. Renton

School of Engineering
University of Aberdeen
Aberdeen AB24 3UE
United Kingdom

(Accepted for Publication in *Materials Science and Engineering A*, Dec 2011)

Abstract

The effect of ageing temperature and holding time on the precipitation of secondary phases and the mechanical properties of a 25Cr-6.7Ni-0.32N-3.0Mo-2.5W super duplex stainless steel is examined. The ageing temperature was varied from 600 to 900 ^{o}C and the holding time was varied from 1 to 240 minutes. Two types of Cr and Mo enriched intermetallic phases, sigma (σ) and chi (χ), were found to precipitate preferentially at the ferrite/austenite interface and within the ferrite grain. The precipitation of the χ-phase occurred preferentially before the σ-phase. The concentration of these secondary phases, which was quantified by a combination of microscopy and image analysis, increases with increasing ageing temperature and holding time, leading to significant reduction in the uniform strain and enhancement of the modulus, hardness and yield and tensile strengths. The measured concentration of the precipitated sigma phase is in agreement with the prediction by the Johnson-Mehl-Avrami kinetic model.

Keywords
A: Electron microscopy, mechanical characterisation, hardness measurement.
B: Stainless steel, intermetallics.
C: Isothermal ageing.
D: Phase transformation, precipitation, hardness, failure, strength

[1] Corresponding author. Email: a.r.akisanya@abdn.ac.uk. Fax: +44 1224 272495

1 Introduction

The duplex family of stainless steels (DSS) contain a mixture of ferrite and austenite and combine some characteristics of each of these phases. The chemical composition and duplex microstructure of approximately equal volume fractions of ferrite and austenite found in DSS result in high strength and good resistance to corrosion, abrasion and wear [1]. It is not surprising therefore that different grades of DSS are increasingly used to store and transport highly corrosive fluids and gases in a wide range of industry sectors. Further enhancement to the mechanical properties and/or corrosion resistance of DSS can be achieved by appropriate addition of alloying elements, e.g. chromium, nickel, molybdenum, nitrogen, copper and tungsten.

DSS are usually categorised by the nominal percentage weight of the chromium (e.g. 18Cr, 22Cr and 25Cr) and other main alloying elements which result in different Pitting Resistance Equivalent Number (PREN). The PREN is a measure of a material's intrinsic resistance to pitting corrosion and it is determined from the element composition (in percentage weight) [2, 3]:

$$PREN_a = \%Cr + 3.3\,(\%Mo + 0.5\,\%W) + a\,\%N \quad (1)$$

where *a* is a material constant whose value ranges between 16 and 32. DSS with PREN greater than 40 are classed as super duplex stainless steel (SDSS). The greater the PREN, the better is the pitting corrosion resistance. The addition of chromium confers passivity on the iron base alloy thus enhancing the corrosion resistance.

Although, the alloying of DSS can enhance the mechanical properties and corrosion resistance, the benefits of alloying can also be associated with microstructure or phase instability leading to matrix impoverishment of the main alloying elements (e.g. chromium, molybdenum, and niobium) and formation of secondary phases at elevated temperature associated with processing, fabrication or operation. Several precipitation reactions can occur when DSS or SDSS is annealed in the temperature range of 600 to 1300 °C, leading, for example, to the formation of secondary phases such as sigma (σ), Chi (χ) secondary austenite (γ_2), carbides (e.g. $M_{23}C_6$), and

nitrides (e.g. Cr_2N) [4 - 7]. Among all these phases, σ-phase is the most important because it significantly reduces the ductility and toughness of duplex steels [7 - 12]. The sigma phase tends to precipitate at the ferrite-austenite interface which has a high interfacial energy that favours such precipitation or at twin boundaries within the austenite phase. An inappropriate heating cycle can cause the precipitation of secondary phases with a consequential reduction in toughness and corrosion resistance that may severely affect the reliability of products made from duplex steel as demonstrated, for example, by Bakajova et al. [7] and Ghosh and Mondal [12]. These failures and the development of new alloys mean there is a need to relate the manufacturing and fabrication (e.g. welding) processes of duplex stainless steels and the service conditions to the mechanical properties and performance for better materials selection in engineering design.

Several authors, e.g. [4 - 16], have studied the effects of ageing and heat treatment on the microstructure, impact strength and corrosion of different grades of stainless steel, including DSS. Many of these studies focused on 22Cr DSS, e.g. [7-9, 12-13, 15-16], with a smaller number of studies on 25Cr SDSS grades. Martins and Casteletti [11, 17] examined the ageing process and the effects on microstructure evolution and impact toughness of cast 25Cr-7.2Ni-0.52Mn-3.8Mo DSS (ASTM A890/A890M Gr 6A) over a temperature range of 500 ^{o}C to 1150 ^{o}C after a holding time of 2 hours while Dyja and Stradomski [18] examined cast 25Cr-6.3Ni-1.3Mn-3Mo DSS over a temperature range of 480 to 520 ^{o}C for a holding time of 4 hours.

These studies were on cast super duplex with coarser grain sizes than those in wrought SDSS. The processing differences between the cast and wrought duplex generally result in more distinct micro-segregation in a cast structure with attendant difference in phase evolution and resulting mechanical properties between the cast grade and wrought grade. Furthermore, the grades of the 25Cr SDSS which have been studied by other authors either have no tungsten (e.g. UNS S32750) or contain tungsten up to a maximum of 1 wt% (e.g. UNS S32760). However, the grade considered in the current study (i.e. 25Cr-6.7Ni-0.32N-3.0Mo-2.5W) has a higher concentration of tungsten, up to 2.5 wt%; tungsten is known to increase the tendency of sigma phase precipitation. It can therefore be inferred that the phase composition

and resulting mechanical behaviour following heat treatments of the 25Cr-6.7Ni-0.32N-3.0Mo-2.5W and that of other grades of 25Cr DSS that contain tungsten less than 1 wt% would be different.

In the current paper, we examine the isothermal ageing of a wrought 25Cr-6.8Ni-3.0Mo-2.5W-0.32N super duplex stainless with $PREN_{16}$ in the range 42-44. The microstructure and phase evolution during the isothermal ageing of the material in the temperature range of 600 - 900 °C for holding time ranging from 1 min. to 4 hours is examined. The aim is to characterise and quantify the secondary phases, in particular, the sigma and chi phases, as a function of the ageing temperature and duration, and the consequent effects on the mechanical behaviour, mainly the hardness and the uniaxial tensile properties. The measured sigma phase is compared with existing phase transformation kinetics model.

2 Experimental Procedure

2.1 Material

The chemical composition of the SDSS examined is shown in Table 1 [19]. The as-received material was a commercial wrought seamless steel pipe with outside diameter of 178 mm and 14 mm wall thickness. The pipe had been manufactured following a plug mill seamless pipe fabrication process.

2.2 Characterisation of microstructure and phases

Rectangular cuboid test specimens, each measuring 10 mm x 10 mm x 5 mm, were machined from the pipe; the 10 mm x 10 mm cross-section was in the radial – longitudinal plane of the pipe. Adequate coolant was used during machining to minimise the effects of the generated heat generated on the microstructure. The specimens were solution annealed at 1050°C for 1 hour followed by water quenching to produce a balanced ferrite/austenite microstructure. Subsequently, the specimens were aged at temperatures of 600, 700, 800 and 900 °C for duration of 1, 5, 10, 20, 40, 80 and 240 minutes, followed by quick quenching in water, and then left to cool in air to ambient temperature.

On completion of the annealing process, the specimens were hot mounted in phenolic resin at 150 ^{o}C and 20.7 MPa using a Buhler mounting press, and then grinded and polished with diamond pastes in a three-stage process using a Buhler Motopol 2000 grinder/polisher. The three stages were: (i) application of 240 grit silicon carbide paper using water as a lubricant for 5 minutes; (ii) utilization of 6 μm diamond suspension with a soft integrity disk for 5 minutes; and (iii) polishing using micro aluminium polishing suspension with a micro-cloth for 10 minutes to produce a polished microstructure.

The microstructure and phase composition were analysed with scanning electron microscope (SEM) using the back scattered electron signal (BSE) and energy dispersive X-ray (EDX) spectroscopic analysis. Further quantitative metallographic studies were also performed using image-analysis toolbox of Clemex Vision Lite imaging system to quantify the volume fractions of the individual phases in accordance with ASTM E1245 [20].

2.3 Hardness and uniaxial tensile tests

The effects of the ageing process on the Vickers hardness and the uniaxial tensile stress-strain response were determined. The hardness tests were conducted on the same specimens used for the microstructure studies.

The uniaxial tensile specimen geometry was a solid circular cylinder with 5 mm diameter and a gauge length of 50 mm. The specimens were machined from the pipe's wall thickness along a direction parallel to the longitudinal axis making appropriate use of coolant to ensure the heat generated during machining did not affect the microstructure. The specimens were solution annealed and subsequently isothermally aged as described above.

Uniaxial tensile tests were conducted at ambient temperature in displacement control using an Instron screw-driven testing machine at a crosshead speed of 0.5 mm/min which is equivalent to a nominal strain rate of $1.7\times10^{-4}\,s^{-1}$. Two 5 mm-gauge post yield strain gauges (type YFLA-5[2]) placed diametrically opposite each other were

[2] Manufactured by Tokyo Sokki Kenkyujo Co. Ltd

attached to the specimen at mid length and orientated in the loading direction. Two dummy gauges were used to ensure temperature compensation on the measured strain. The use of the strain gauges provide accurate strain readings up to the onset of unstable deformation associated with necking and also enable an accurate determination of the modulus. The applied load and the axial strain were continuously monitored and recorded using a computerised data logger.

3 Results and Discussion

3.1 Microstructure and phase evolution

The microstructure of the as-received and solution annealed material is shown in Figure 1. It indicates, as expected, the dual-phase (δ-ferrite and γ-austenite) microstructure with no secondary phases present. The ferrite appears darker than the austenite on the micrograph. Quantitative analysis of the microstructure using Clemex image processing toolbox gave an area fraction of 48% ferrite and 52% austenite. This is consistent with the expected 50:50 ferrite to austenite volume fraction.

No precipitation of any secondary phases was observed after annealing at a temperature of 600 ^{o}C for 240 minutes. At higher temperature, two main intermetallic phases were detected: chi (χ) and sigma (σ); see Figure 2.

The χ-phase precipitates from the ferrite prior to the σ-phase precipitation; with the χ-phase occurring preferentially at ferrite/austenite interfaces and at ferrite/ferrite grain boundaries (see, for example Figures 2a,b). With longer holding time, a eutectoid-type reaction of ferrite leads to the precipitation of the σ-phase at the ferrite-austenite boundary; this however subsequently penetrates the ferrite (Figure 2). The χ-phase acts as the preferential sites for the σ-phase nucleation [10]. Once the σ-phase is precipitated, both secondary phases co-exist but the σ-phase grows very quickly with increasing ageing time and subsequently some of the existing χ-phase are transformed to σ-phase. The transformation of the χ-phase and ferrite to σ-phase takes place with increase in ageing time (Figure 2c,d). This is in agreement with similar observation in 22Cr cast DSS [9, 13]. The minimum holding time before any noticeable precipitation of the secondary phases is observed is a

function of the temperature: we note that the χ-phase precipitated after 1 minute at 800 and 900 °C and after 10 minutes at 700 °C. Martin and Casteletti [17] obtained an incubation time of 5 min. before the onset of the precipitation of secondary phases in 25Cr-7.2Ni-0.52Mn-3.8Mo-0.74W DSS (ASTM A890/A890M Gr 6A) aged between 800 – 950 °C. The precipitation of the secondary phases occurred sooner in the material used in this study most likely as a result of the greater tungsten content (about 2.6 wt%); tungsten accelerates the precipitation of secondary phases at temperatures below 900 °C.

An increased amount of the secondary phases was observed at prolonged hold time (> 80 minutes) and high temperatures (≥ 800 °C), see Figures 2c and 2d. This is attributed to the enhanced diffusion of solute elements, i.e., Cr, Mo, Si, etc. from the ferrite phase to the ferrite-austenite boundaries as the temperature increased to 900 °C.

Chemical microanalysis of the individual phases was carried out with energy dispersive X-ray system (EDX) coupled to the SEM. The SEM-EDX has X-ray beam diameter of 1 μm. Due to the sub-micron size of the χ-phase (see Figure 2), the use of the SEM-EDX to characterise the element composition within this particular phase involves a tedious and time consuming process to ensure the X-ray beam is focused appropriately at the target location. SEM-EDX has been successfully used by other authors to characterise the element composition of χ-phase and σ-phase in 22Cr DSS [12, 15].

Figure 3 shows typical EDX results obtained in the current study for the specimen aged at 900 °C for 20 minutes. The results indicate that the σ-phase is rich in both Cr and Mo, while the χ-phase is depleted in Cr but richer in Mo than the σ-phase. The quantitative data of the composition of the main elements are summarized in Table 2 as an average for three nominally identical measurements. In comparison to the ferrite and the austenite, the χ and σ phases are much richer in W and Mo, and much depleted in Ni. The composition of W in the 25Cr SDSS aged at 900 °C for 20 minutes was found to be 16.17 wt% in the χ-phase, 9.07 wt% in the σ-phase and 4.85 wt% in the ferrite. During the precipitation of the σ-phase, Cr is absorbed in the

phase while Ni is rejected to the adjacent ferrite and austenite. The EDS results shown in Figure 3 and Table 2 confirm that the σ-phase is Cr-rich and depleted in Ni. The increased concentration of W in the χ-phase is due to the slow diffusion of tungsten in comparison to other elements in the composition. Consequently, W atoms would not diffuse towards the ferrite fast enough to form the σ-phase. Instead, W accumulates at the phase boundary encouraging the early precipitation of χ-phase while suppressing the σ-phase. These results shown in Table 2 are consistent with those reported for 22Cr DSS by other researchers, e.g. [9, 16]. The precipitation of the σ-phase depletes the ferrite of the main solid solution strengtheners, e.g. Cr and Mo, resulting in decrease in material strength and ductility as will be shown later.

3.2 Phase composition

The area fraction of the secondary phases at the different ageing temperatures and holding times was determined by quantitative metallographic analysis based on the grey levels of the microstructural constituents using Clemex image processing toolbox in accordance with ASTM E1245 [20]; the result**s** are shown in Figure 4**.** After an initial increase in the area fraction of the χ-phase, it decreased again, suggesting that χ-phase is metastable in the grade of 25Cr SDSS considered. The χ-phase is consumed in the σ-phase precipitation after becoming completely surrounded by the σ-phase; this is evident in the reduction of the area fraction of the χ-phase as the holding time increases, especially at 900 ^{o}C. There is a rapid increase in the concentration of the σ-phase after about 10 minutes of annealing at a temperature of 700 ^{o}C and higher. For ageing at 900 ^{o}C (Figure 4c), the concentration of the χ-phase decreased from about 7.5% after 10 minutes to about 2.2% after 240 minutes, while the corresponding concentration of the σ-phase increased from 1.8% to 23% during the same time interval. As the ageing temperature approached 900 °C, we observed a more rapid increase in the rate of σ-phase precipitation with increasing holding time and temperature. At temperature above 1000 ^{o}C, the concentration of the σ-phase should start to decrease as the secondary phases are transformed back to ferrite [17].

Although there is a much faster increase in the precipitation of the σ-phase at temperature above 700 ^{o}C and holding time above 10 mins, the rate of growth of the secondary phases in the material considered in this study is lower than for similar 25Cr SDSS with no tungsten. The slower growth rate of the secondary phases may be due to the lower diffusion rate of tungsten. Thus tungsten can delay the precipitation of σ-phase and encourage the precipitation of χ-phase with a higher nucleation efficiency and lower growth rate than the σ-phase and ensures that available nucleation sites are occupied [21].

In addition to the ageing temperature, alloying elements and holding time, there are other parameters that affect the transformation of ferrite to sigma phase and secondary austenite, e.g. the element composition, ferrite grain size and volume fraction, solution annealing temperature and pre-ageing cold working. Thus there is no universal kinetic model that adequately captures the effects of all these parameters on the evolution of the secondary phases during isothermal ageing. However, there is evidence that Johnson-Mehl-Avrami (JMA) model [22] which was developed to describe the kinetics of crystallisation can be used to describe how ferrite transforms to σ-phase, for example, in weld metals [23, 24] and 22Cr DSS [25]. The measured concentration of the σ-phase in the current study is compared with the predictions by JMA model.

According to JMA model, if the transformation occurs under isothermal conditions and the nucleation is random with a constant nucleation frequency, the fraction, *x*, of the initial phase that is transformed at time *t* is given by [22]

$$x = 1 - \exp\left(-At^{n}\right) \qquad (2)$$

where $A = A_o e^{-Q/RT}$ is the reaction rate constant with depends on ageing temperature *T*, universal gas constant *R* and the activation energy *Q*, and *n* is the Avrami material constant. In the current study the initial phase is ferrite and this is transformed primarily to σ-phase; *x* is therefore the fraction of ferrite that is transformed to σ-phase.

If the transformation obeys the JMA model, a plot of ln[ln(1/(1-x)] versus ln(t) should be linear with a slope of n and an intercept of ln(A). Such a plot is shown in Figure 5 for the measured concentration of the σ-phase in the current study. We note that the transformation of ferrite to σ-phase in the current study obeys the JMA model. The Avrami material constant was determined to have values of n = 0.89, 0.92 and 0.95 for ageing temperatures 700, 800 and 900 ^{o}C respectively, and the corresponding reaction rate constant A = 0.090, 0.12 and 0.24. Thus, the temperature dependence of n is therefore relatively small. Sasikala et al. [24] showed that the value of n for AISI 316(N) austenitic stainless steel weld metal is independent of temperature between 550 and 650 ^{o}C, while Lara et al. [25] showed that the value of n for a 22Cr DSS is temperature dependent: n = 0.59 at 700 ^{o}C and n = 0.77 at 800 ^{o}C.

The JMA exponent, n, is often associated with different types of nucleation and growth conditions, and it provides an indication of the kinetics responsible for the transformation: n close to 1 implies rapid transformation while much lower values n imply slow transformation. The calculated n values range from 0.89 to 0.95 and thus indicate a rapid transformation of the secondary phases. Recall, that the presence of the tungsten encourages early precipitation of the χ-phase at every possible nucleation site, which then gets transformed rapidly into the sigma phase. The nucleation and growth of the secondary phases are diffusion controlled at all the temperatures considered, hence the relatively temperature-independent value of n obtained in this study.

The estimated values of n and A given above are used to compare the predicted proportion of ferrite transformed to σ-phase to the measured proportion in Figure 6. There is a reasonable agreement between the measured and the predicted fraction of transformed ferrite for the 25Cr DSS considered in this study.

3.3 Hardness

In order to assess the effect of secondary phases on the hardness and uniaxial tensile properties, the solution annealed as-received material and four combinations of ageing temperature and time were considered, to ensure a wide range of the amount of secondary phases. The chosen ageing temperatures and times and the corresponding concentration of the secondary phases are given in Table 3. Recall

that the as-received material after solution annealing has neither σ- nor χ-phase. The concentration of the σ–phase considered ranged between 0% and 23% while concentration of the total secondary phase (σ plus χ) was between 0% and 25.5%, see Table 3. With the exception of the ageing at 900 ^{o}C for 20 minutes, the secondary phase in all the cases considered for hardness and uniaxial tensile test consisted of predominantly the σ–phase.

Three hardness measurements were taken using three nominally identical specimens. In all cases, the three measurements were identical to within a few percent. The average hardness for three nominally identical specimens are shown in Figure 7 as a function of the area fraction of the total secondary phases. The hardness increases with increasing concentration of secondary phases. A 25% area fraction of the secondary phases increased the hardness of the as received 25Cr wrought DSS by 44%. The hardness of a 25Cr DSS containing 0.74 wt% of tungsten only increased by 15% when the area fraction of the secondary phases was increased from zero in the solution annealed state to 25% after ageing [17]. The hardness of the σ–phase is significantly greater than that for the χ-phase, ferrite or austenite; in fact the hardness of the σ–phase is almost twice as high as that for austenite [19]. As the secondary phases are predominantly the σ–phase, the increase in the hardness observed in the present study is therefore associated with increasing concentration of the σ–phase.

3.3 Uniaxial tensile stress–strain response

The uniaxial tensile stress-strain response of the 25Cr SDSS was used to examine the effects of the σ-phase on the ductility and strength. Figure 8 shows the effects of the secondary phases on the stress-strain response. At low concentration of the σ-phase (equal or less than about 5% area fraction), the stress-strain response is almost elastic-ideally plastic with negligible strain hardening, just as for the solution annealed as-received material. However at higher concentration of σ-phase, we noticed an appreciable strain hardening before failure but with significantly reduced plastic deformation.

The failure modes changes from being ductile at low concentration of secondary phases (less than 15%) to brittle at higher concentration of secondary phases, see Figure 9. Necking occurred within the uniform diameter gauge length of the specimens, but away from the location of the 5 mm long strain gauge (see Figure 9). Consequently, the strain gauges were able to accurately record the level of deformation up to the onset of necking. Once necking occurred the strain gauges were unable to accurately record the strain associated with the localised and non-uniform deformation. Thus the stress-strain curves shown in Figure 8 are up to the onset of necking and the end of uniform deformation. The magnitude of the uniform strain decreases with increasing area fraction of the secondary phases.

The uniaxial tensile properties are shown in Figure 10. The Young's modulus and the yield stress are determined using the stress – strain data before the onset of necking; this was accurately measured by the strain gauge. For area fraction of the secondary phases which is equal to or less than about 7%, there is insignificant change in the Young's modulus, uniform strain, tensile strength (UTS) and the 0.2% proof stress ($\sigma_{0.2}$). At higher concentration of secondary phases, we observe a significant increase in the Young's modulus, 0.2% proof stress and the UTS (Figure 10); this is consistent with corresponding increase in the hardness (see Figure 7). However, there is a significant decrease in the uniform strain with increasing concentration of the secondary phases greater than 7% (Figure 10c). The values of both the 0.2% proof stress and UTS when there was about 26% secondary phases were 23% greater than the corresponding values for the as-received solution annealed material, while the corresponding uniform strain decreased by 88%.

The ductility was determined from the gauge length at fracture (obtained by fitting the broken specimens together and measuring the length) L_f and the initial gauge L_o :

$$\text{Elongation} = \frac{L_f - L_o}{L_o} \times 100 \qquad (3)$$

The effect of the secondary phase on the ductility is shown in Figure 10d. We note a significant reduction in ductility from 33% when there was no secondary phase to 15% when there was about 26% concentration of secondary. In contrast, a 22Cr

DSS with no tungsten was shown to retain considerable amount of ductility when aged at 900 ^{o}C for up to 120 minutes [12].

The processing of the higher tungsten 25Cr SDSS considered in this paper and the service application therefore requires a compromise between increased stiffness and strength and reduced ductility associated with the prolonged isothermal ageing at elevated temperature. The loss of ductility is of particular significance for welding procedures, where temperature and time must be carefully considered to avoid material property gradients across the heat affected zone and resultant detrimental stress concentrations. This phenomenon may be further compounded by the known corrosion resistance problems caused by intermetallic precipitation.

The alloying elements of the SDSS considered in this study make it suitable for oil and gas well completion systems and transportation of highly corrosive hydrocarbons that contain a combination of CO_2, H_2S and chlorides. The results presented in this paper provide the interrelationship between isothermal ageing conditions, microstructure and mechanical properties of 25Cr-6.8Ni-3.0Mo-2.5W-0.32N SDSS which would aid better design of and material selection for subsurface, subsea, and production equipment used in high pressure and high temperature oil and gas wells. The effect of heat treatment on the corrosion resistance of the SDSS in typical environment found in oil and gas wells is part of an ongoing research by the authors.

4 Conclusions

When super duplex stainless steels are exposed to temperatures below the solution annealing temperature, the metastable thermodynamic balance is disturbed, causing the material to seek a more stable thermodynamic state through the precipitation of intermetallic phases. When the wrought super duplex stainless steel used in the current study was aged at 600, 700, 800 and 800 °C, two major intermetallic phases were detected: chi (χ) and sigma (σ). The χ-phase precipitates at ferrite/ferrite grain boundaries prior to the σ-phase precipitation and occurs preferentially at ferrite/austenite interfaces and at ferrite/ferrite grain boundaries. After an initial increase in the area fraction of the χ-phase, it decreased again, suggesting that the

χ-phase is metastable in this grade of SDSS. The secondary phases precipitated sooner in the material in comparison to other grades of 25Cr DSS due to increased amount of tungsten in the composition.

The concentration of the secondary phase less than about 7% has no little or no effect on the UTS, 0.2% proof stress, Young's modulus, and the uniform strain of the material. However, increasing concentration of the secondary phase which is associated with higher annealing temperature and/or hold time significantly reduces the ductility and enhances the hardness, modulus and the yield and tensile strengths.

Acknowledgements

The authors acknowledge the experimental assistance of Mark Gourlay, Alastair Robertson and Irene Logan of the University of Aberdeen, School of Engineering Central Workshop, and are also grateful to John Still of the School of Geosciences for assistance with the SEM work.

References

[1] J.O. Nilsson, Mater. Sci. Technol. 8 (1992) 685–700.

[2] H. Hanninen, J. Romu, R. Ilola, J. Tervo, A. Laitinen, J Mater Proc Tech. 117 (2001) 424-430.

[3] R.A. Perren, T.A. Suter, P.J. Uggowitzer, L. Weber, R. Magdowski, H. Bohni, M.O. Speidel, Corr. Sci. 43 (2001) 707-726.

[4] K. Unnikrishnan, A.K. Mallik, Mater. Sci. Eng. A 95 (1987) 259–265.

[5] M. Pohl, O. Strorz, T. Glogowski, Int. J. Mater. Res. 99 (2008) 1163-1170.

[6] L. Duprez, B.D. Cooman, N. Akdut, Steel Res. 10 (2000) 417–422.

[7] J. Bakajova, M. Domankova, R. Cicka, S. Eglsaer, J. Janovec, Mater. Charact. 61 (2010) 969-974

[8] T.H. Chen, K.L. Weng, J.R. Yang, Mater Sci Eng A 338 (2002) 259–270.

[9] T.H. Chen, J.R. Yang, Mater. Sci. Eng. A 338 (2002) 166-181.

[10] J.O. Nilsson, T. Karlsson, A. Wilson, Metall. Mater. Trans. A 31 (2000) 35-45.

[11] M. Martins, L.C. Casteletti, Mater. Charact. 60 (2009) 792-795.

[12] S.K. Ghosh, S. Mondal, Mater. Charact. 59 (2008) 1776-1783.

[13] D.M. Escrib, E. Materna-Morris, R.L. Plaut, A.F. Padilha, Mater. Charact. 60 (2009) 1214-1219.

[14] L. Karlsson, Weld. Res. Council Bull. 438 (1999) 1–23

[15] I. Calliari, M. Zanesco, E. Ramous, J. Mater. Sci. 41 (2006) 7643–7649.

[16] E.M. Jackson, P.E. de Visser, L.A. Cornish, Mater. Charact. 31 (1993) 185–190.

[17] M. Martins, L.C. Casteletti, J. ASTM International 2 (2005) 1-14.

[18] D. Dyja, Z. Stradomski, Arch. Mater. Sci. Eng. 28 (2007) 557-564.

[19] N.C. Renton, Time variant reliability of super duplex stainless steel tubular. PhD thesis, University of Aberdeen, UK, 2007.

[20] ASTM E1245-03. Practice for determining the inclusion or second phase constituent content of metals by automatic image analysis. ASTM 2008.

[21] K. Ogawa, H. Okamoto, M. Igarashi, M. Ueda, T. Mori, T. Kobayashi, Welding International 11 (1997) 14-22

[22] J.W. Christian, The theory of transformation in metals and alloys, in Part I: Equilibrium and General Kinetic Theory, second ed., Pergamon Press, Oxford, 1975.

[23] R. Badji, M. Bouabdallah, B. Bacroix, C. Kahloun, K. Bettahar, N. Kherrouba, Mater. Sci. Eng. A 496 (2008) 447–454.

[24] G. Sasikala, S.K. Ray, S.L. Mannan, Mater. Sci. Eng. A 359 (2003) 86-90.

[25] N.O. Lara, A. Ruiz, C. Rubio, R.R. Ambriz, A. Medina, NDT&E International 44 (2011) 463-468.

List of Figures

Figure 8 Effect of ageing on the uniaxial stress-strain response of three nominally identical specimens. (a) As received after solution annealed: no secondary phases. (b) Aged at 900 ^{o}C for 20 minutes: 5.1% σ-phase and 7.5% χ-phase. (c) Aged at 900 ^{o}C for 80 minutes: 13.1% σ-phase and 2.9% χ-phase. (d) Aged at 900 ^{o}C for 240 minutes: 23.3% σ-phase and 2.2% χ-phase.

Figure 9 The failed specimens. The concentration of the secondary phases is stated beneath each specimen.

Figure 10 Effect of the concentration of the secondary phases on the (a) Young's modulus, (b) ultimate tensile strength, UTS, and the 0.2% proof stress, (c) the uniform strain, and (d) residual elongation after failure.

Table 1: Chemical composition of the investigated UNS S39274 (SM25CRW) duplex stainless steel. Data obtained from [19]

Chemical Composition (wt%)										
C	**Si**	**Mn**	**P**	**S**	**Cu**	**Ni**	**Cr**	**Mo**	**W**	**N**
0.02	0.36	0.49	0.028	< 0.015	0.49	6.83	24.5	3.27	2.61	0.32

Table 2: Chemical composition of various phases obtained by EDS analysis after ageing UNS S39274 (SM25CRW) duplex stainless steel at 900 ^{o}C for 20 minutes (wt%)

Elements	**Ferrite**	**Austenite**	**χ-phase**	**σ–phase**
Cr	23.13 ± 0.77	23.79 ± 1.22	21.73 ± 1.84	26.25 ± 1.45
Mo	2.89 ± 0.09	4.44 ± 0.66	10.10 ± 0.22	6.57 ± 0.13
Ni	6.80 ± 0.54	8.23 ± 1.07	3.46 ± 0.05	3.84 ± 0.10
W	4.85 ± 0.19	3.43 ± 0.42	16.17 ± 0.72	9.07 ± 0.03

Table 3: The ageing schedule and amount of secondary phases considered for hardness and uniaxial tensile tests.

Annealing schedule		**Area fraction of individual secondary phases (%)**		**Total area fraction of secondary phases (%)**
Temperature (^{o}C)	**Time (min)**	**σ-phase**	**χ-phase**	
900	20	5.10	7.46	12.56
800	40	5.44	1.50	6.94
900	80	13.10	2.85	15.95
900	240	23.30	2.20	25.50
Solution annealed, as received material		0	0	0

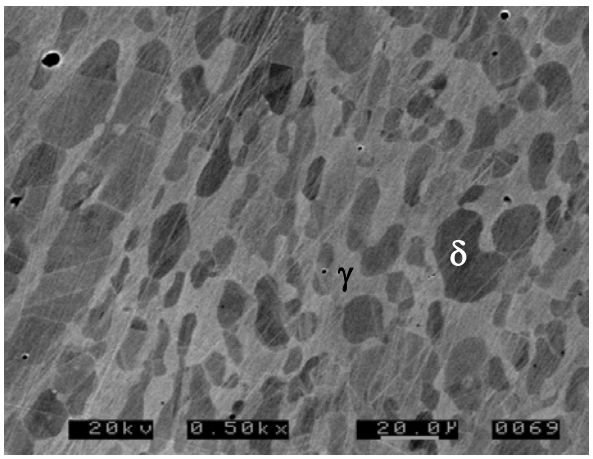

(a)

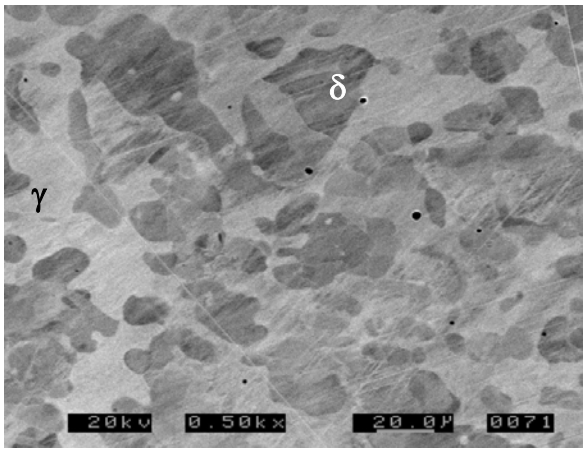

(b)

Figure 1

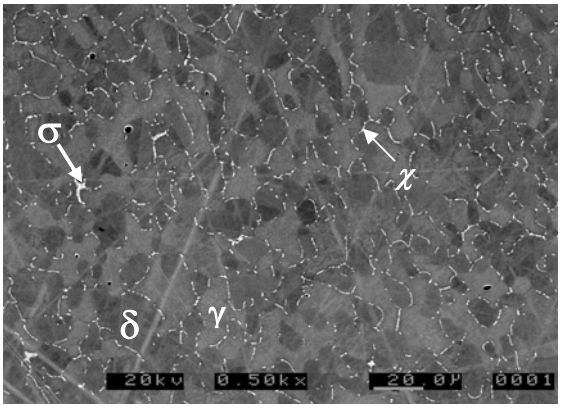

(a)

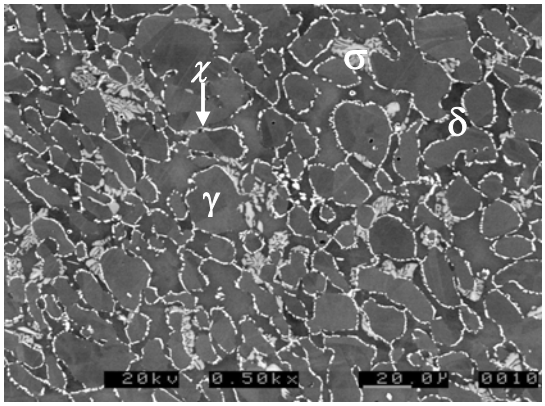

(b)

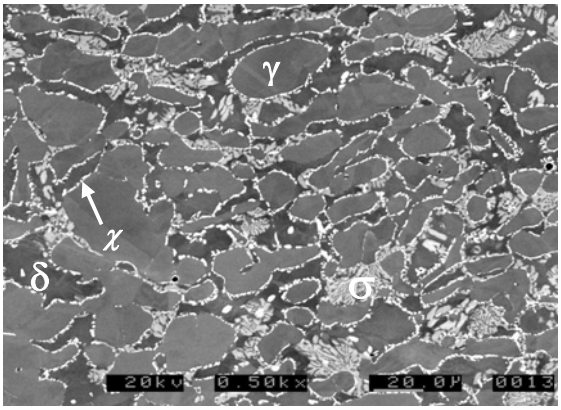

(c)

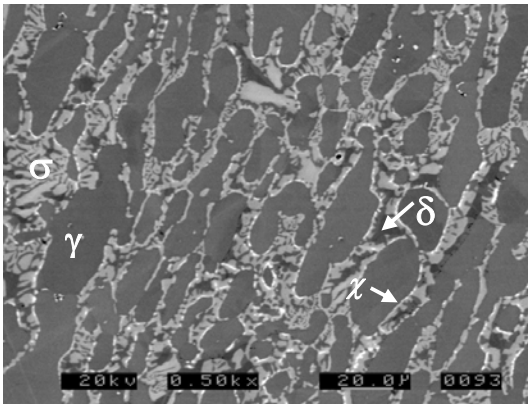

(d)

Figure 2

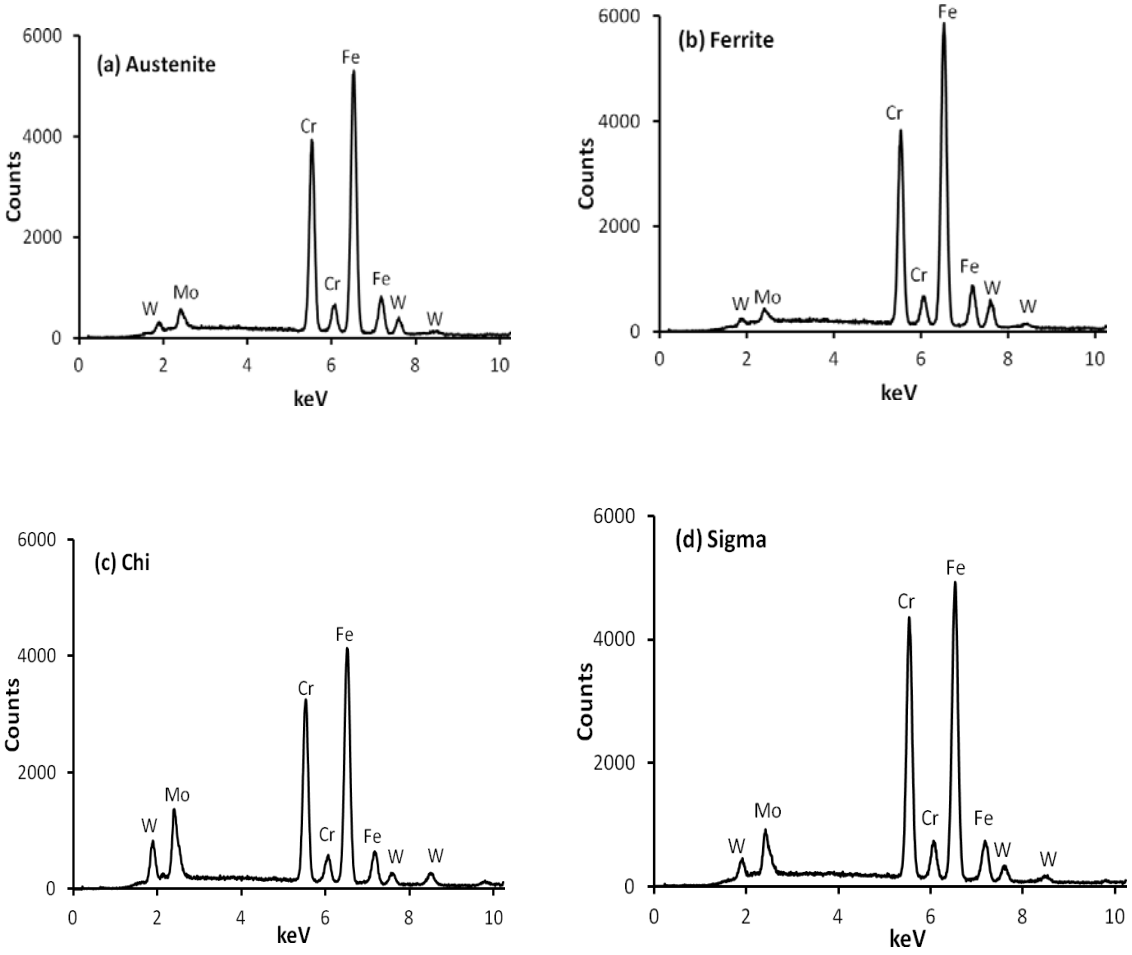

Figure 3

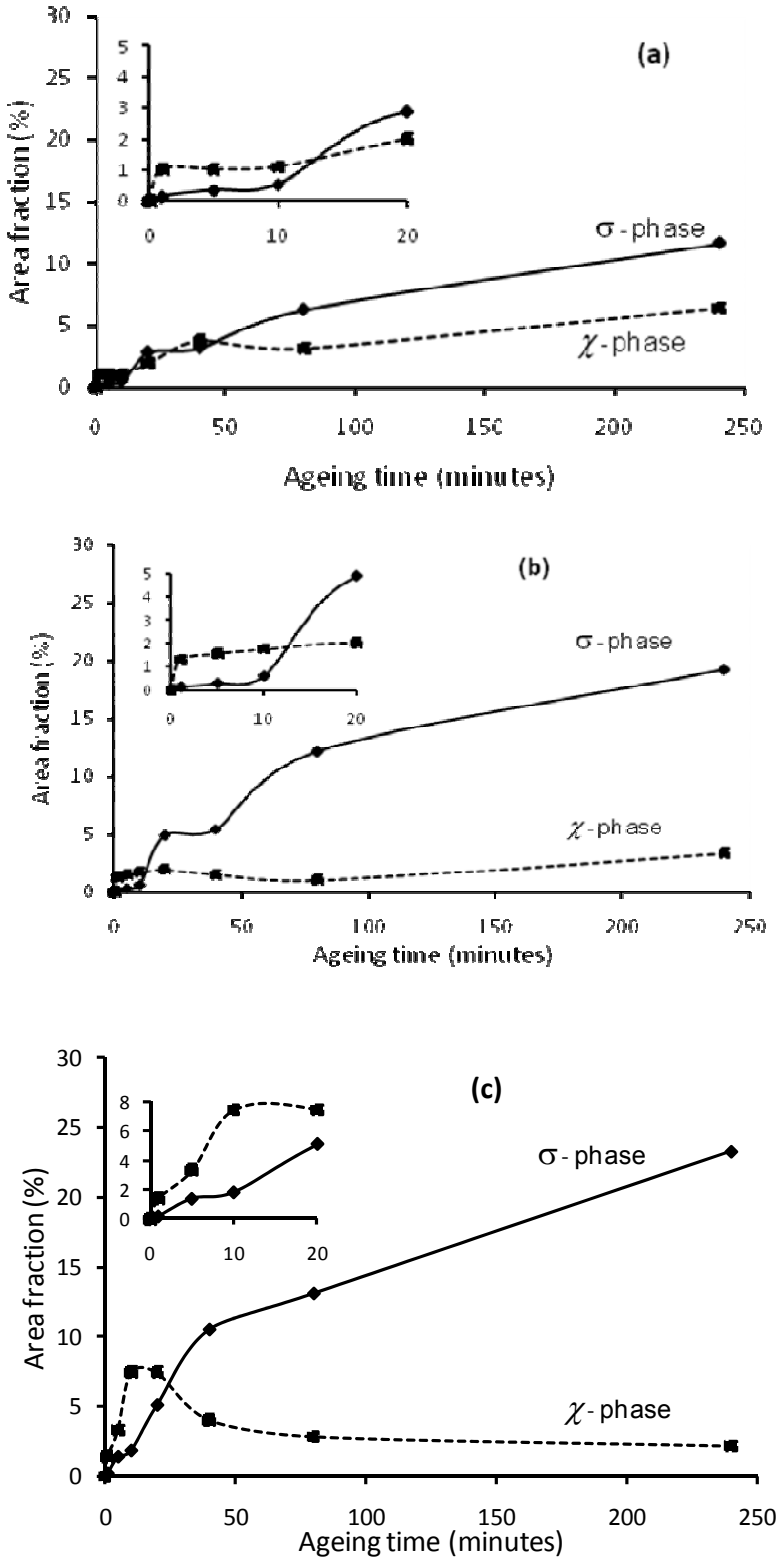
(a)
Area fraction (%)
σ - phase
χ - phase
Ageing time (minutes)
(b)
Area fraction (%)
σ - phase
χ - phase
Ageing time (minutes)
(c)
Area fraction (%)
σ - phase
χ - phase
Ageing time (minutes)

Figure 4

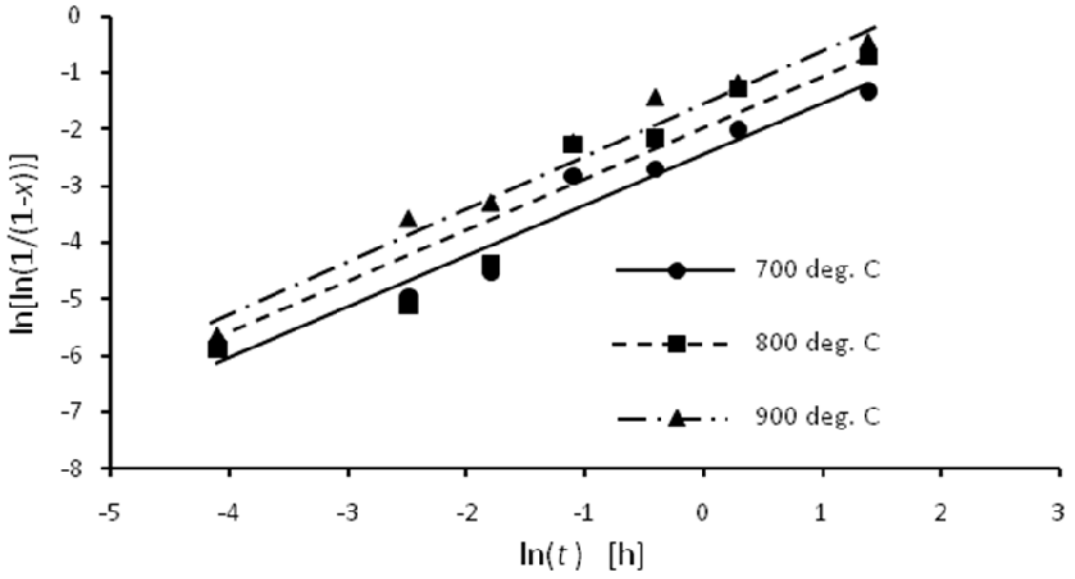
0
-1
-2
-3
-4
-5
-6
-7
-8
ln[ln(1/(1-x))]
-5
-4
-3
-2
-1
0
1
2
3
ln(t) [h]
700 deg. C
800 deg. C
900 deg. C

Figure 5

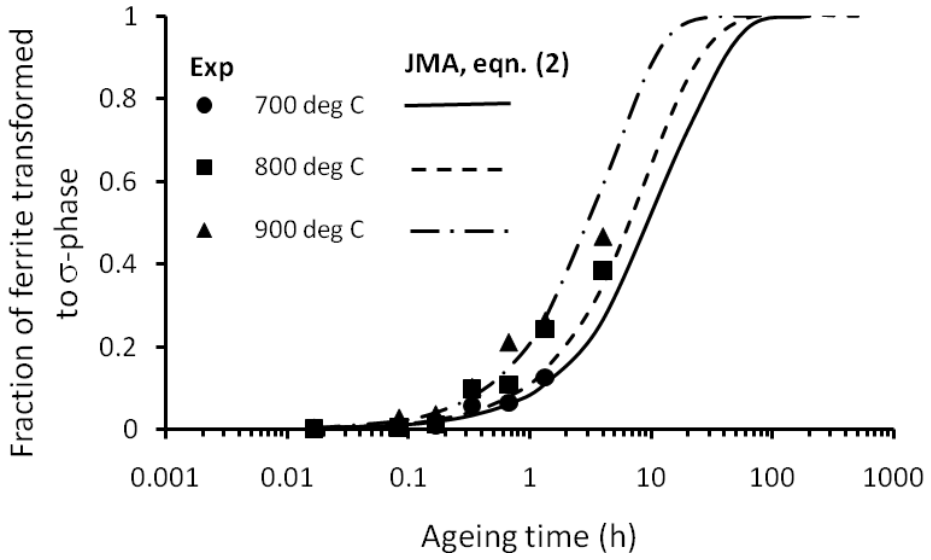
Fraction of ferrite transformed to σ-phase
1
0.8
0.6
0.4
0.2
0
Exp
700 deg C
800 deg C
900 deg C
JMA, eqn. (2)
0.001
0.01
0.1
1
10
100
1000
Ageing time (h)

Figure 6

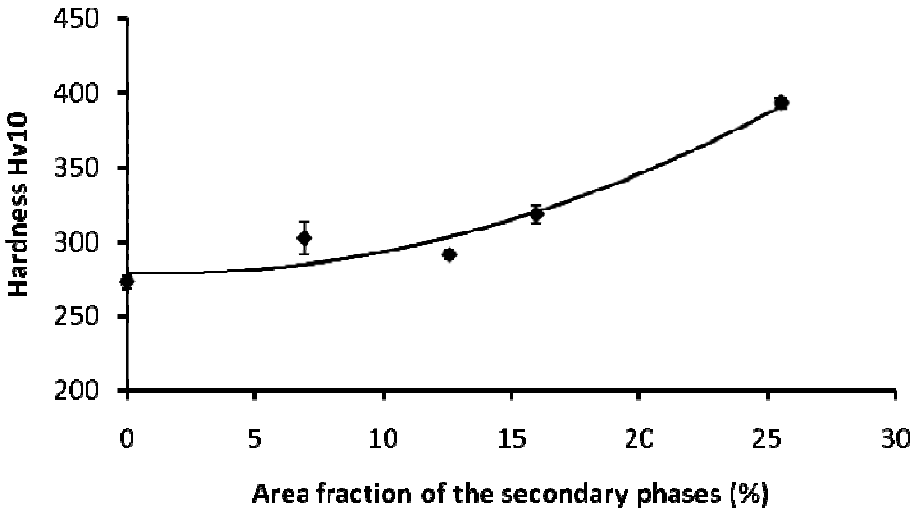
450
400
350
300
250
200
Hardness Hv10
0
5
10
15
20
25
30
Area fraction of the secondary phases (%)

Figure 7

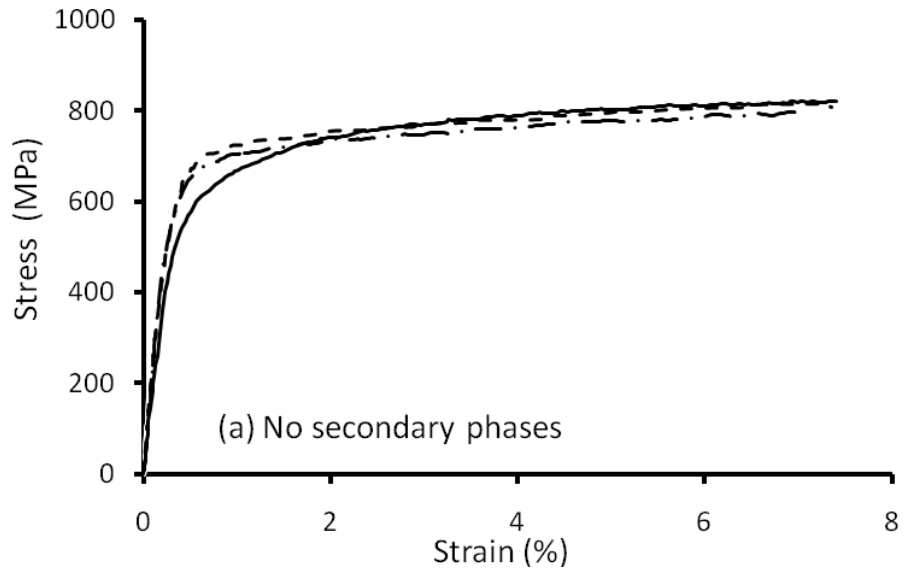
1000
800
600
400
200
0
Stress (MPa)
(a) No secondary phases
0
2
4
6
8
Strain (%)

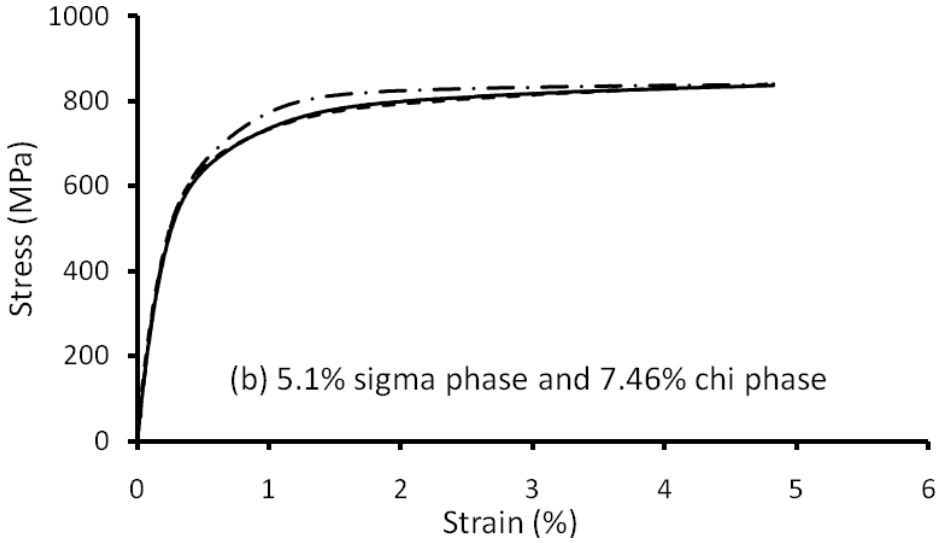
1000
800
600
400
200
0
Stress (MPa)
(b) 5.1% sigma phase and 7.46% chi phase
0
1
2
3
4
5
6
Strain (%)

Figures 8a,b

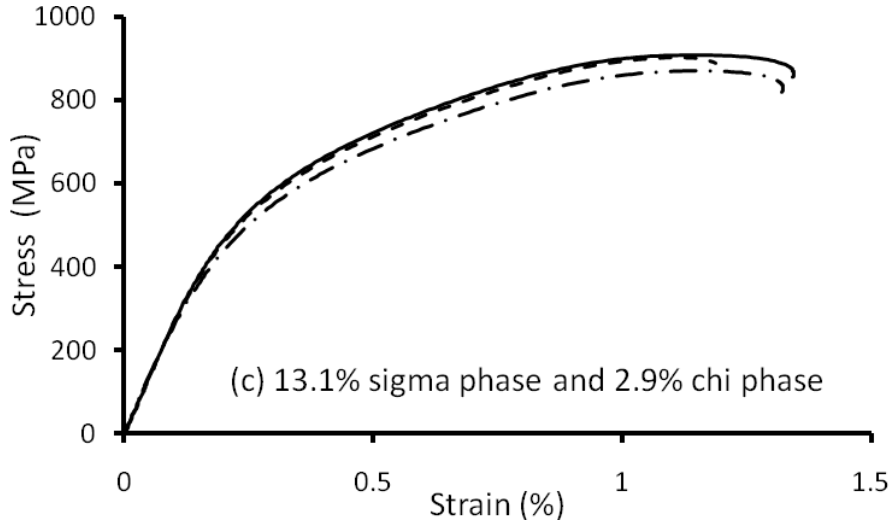
1000
800
600
400
200
0
Stress (MPa)
(c) 13.1% sigma phase and 2.9% chi phase
0
0.5
1
1.5
Strain (%)

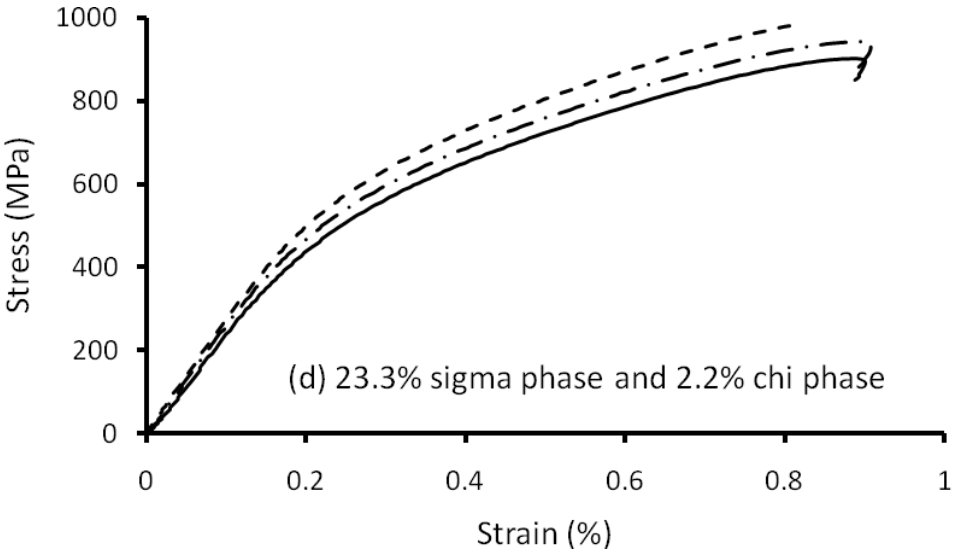
1000
800
600
400
200
0
Stress (MPa)
(d) 23.3% sigma phase and 2.2% chi phase
0
0.2
0.4
0.6
0.8
1
Strain (%)

Figure 8c,d

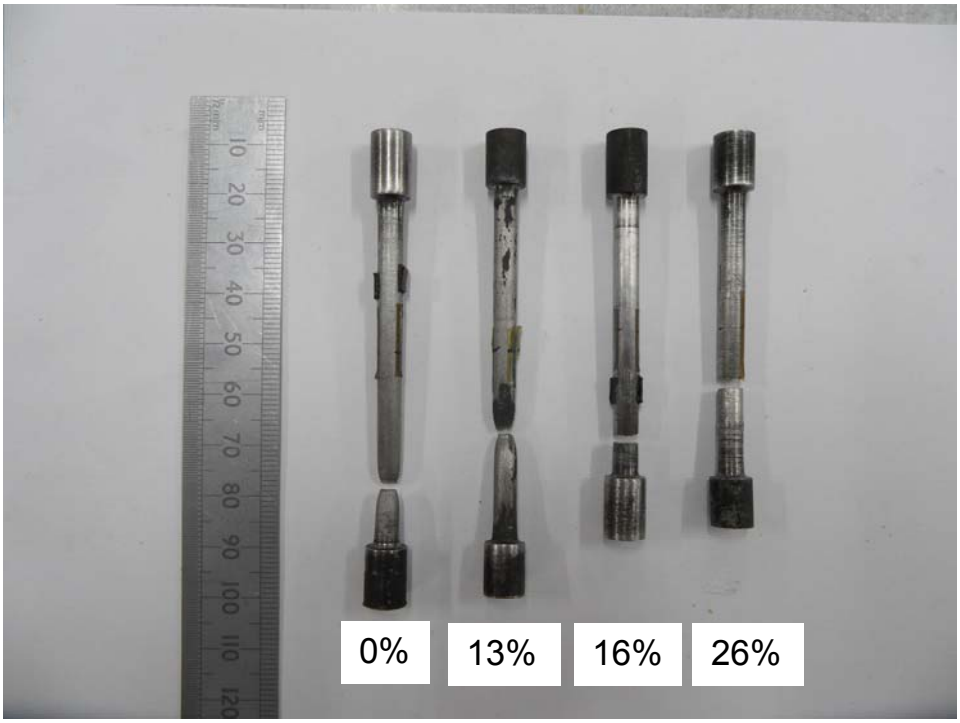

Figure 9

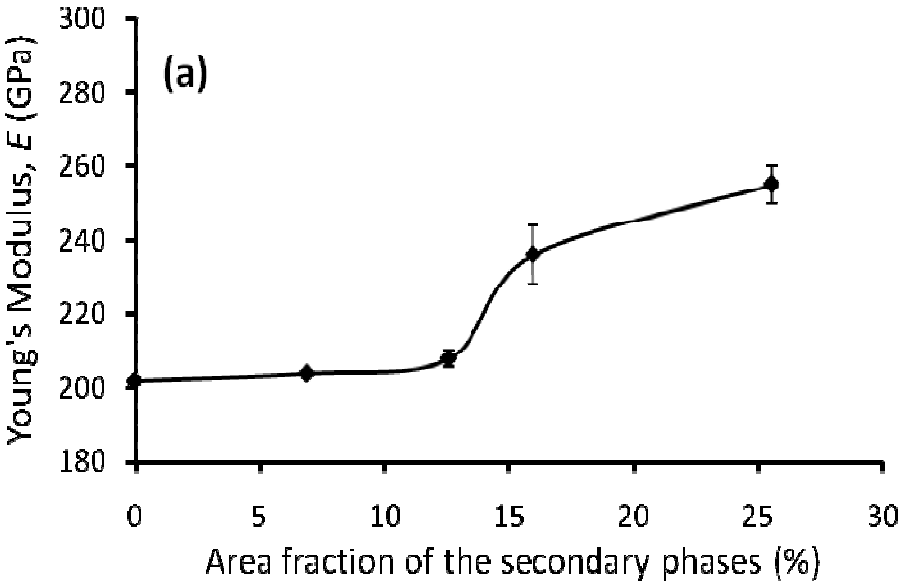
(a)
Young's Modulus, E (GPa)
300
280
260
240
220
200
180
0
5
10
15
20
25
30
Area fraction of the secondary phases (%)

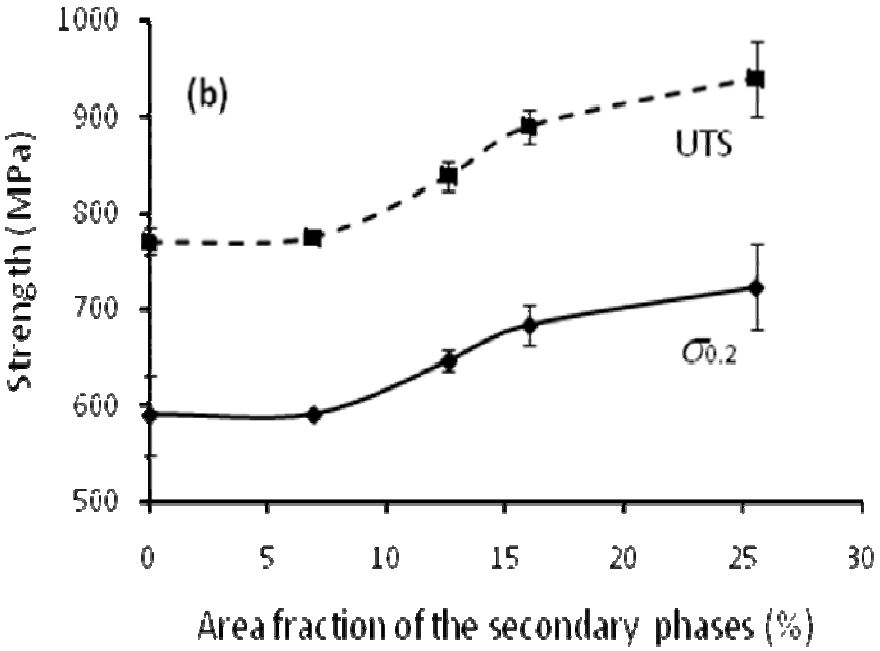
(b)
Strength (MPa)
1000
900
800
700
600
500
UTS
σ0.2
0
5
10
15
20
25
30
Area fraction of the secondary phases (%)

Figure 10a&b

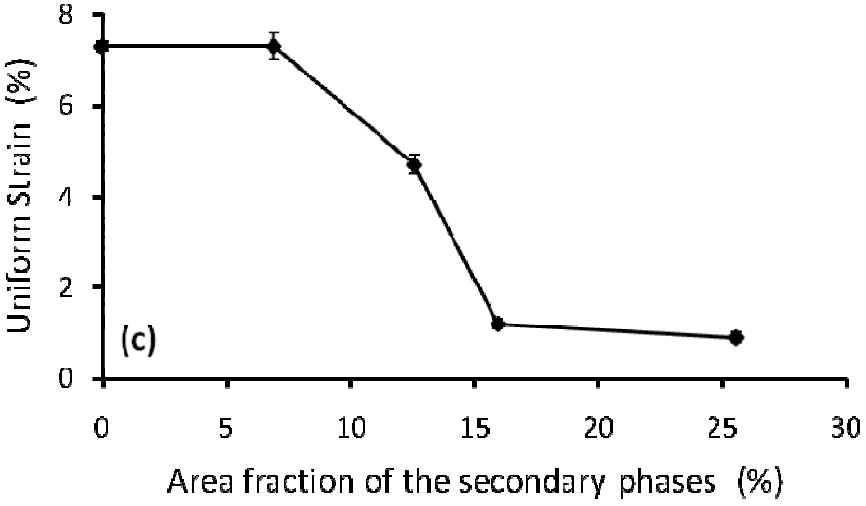
Uniform Strain (%)
8
6
4
2
0
(c)
0
5
10
15
20
25
30
Area fraction of the secondary phases (%)

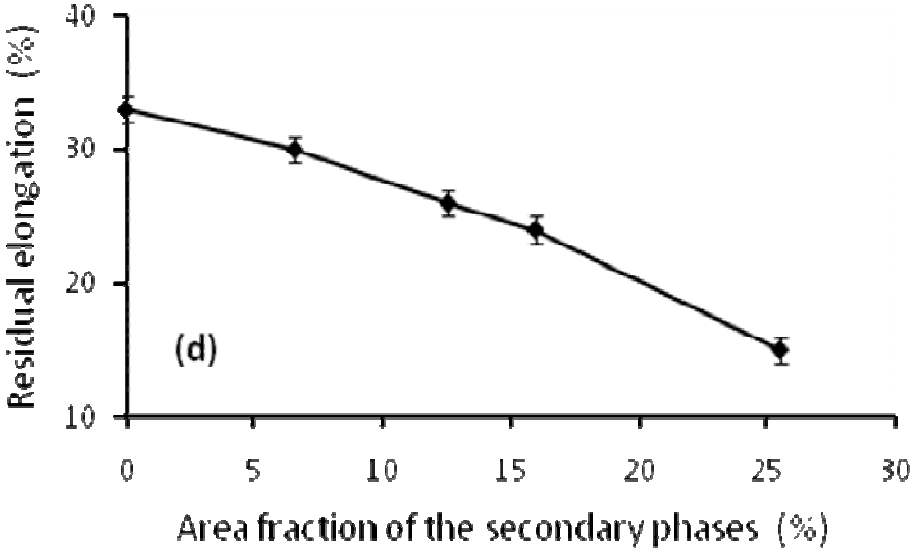
Residual elongation (%)
40
30
20
10
(d)
0
5
10
15
20
25
30
Area fraction of the secondary phases (%)

Figure 10c&d